Identification of Defective Areas in Composite Materials by Bivariate EMD Analysis of Ultrasound

Marco Leo, David Looney, *Member, IEEE*, Tiziana D'Orazio, *Member, IEEE*, and Danilo P. Mandic, *Senior Member, IEEE*

***Abstract*—In recent years, many alternative methodologies and techniques have been proposed to perform nondestructive inspection and maintenance operations of moving structures. In particular, ultrasonic techniques have shown to be very promising for automatic inspection systems. From the literature, it is evident that the neural paradigms are considered, by now, the best choice to automatically classify ultrasound data. At the same time, the most appropriate preprocessing technique is still undecided. The aim of this paper is to propose a new and innovative data preprocessing technique that converts real-valued ultrasonic data into complex-valued signals. This allows analysis using phase synchrony, a robust tool that has been previously employed in brain science for establishing robust features in noisy data. Synchrony estimation is achieved using complex extensions of empirical mode decomposition, a data-driven algorithm for detecting temporal scales, thus facilitating the modeling of nonlinear and nonstationary signal dynamics. Experimental tests aiming to detect defective areas in composite materials are reported, and the effectiveness of the proposed methodology is illustrated.**

***Index Terms*—Aerospace safety, feature extraction, neural networks, pattern recognition, ultrasonic imaging.**

I. Introduction

THE CHALLENGE of guaranteeing reliable and efficient safety checks for engineering structures has received much attention in recent years in many industrial contexts mostly owing to the advances in computer technology, as well as to the emergence of powerful signal processing and learning methodologies [1]–[3]. In particular, this challenge is of crucial importance for a number of industrial applications including manufacturing processes, hazardous waste management systems, inspection and maintenance of aircraft, and electrical power lines where unpredictable behavior, such as poor performance or even unsafe operation, can result from abnormal deviations and/or anomalies in components, sensors, and actuators [4].

Manuscript received September 14, 2010; revised February 8, 2011; accepted February 24, 2011. Date of publication July 14, 2011; date of current version December 8, 2011. The Associate Editor coordinating the review process for this paper was Dr. Shant Kenderian.

M. Leo and T. D'Orazio are with the Institute of Intelligent Systems for Automation, Italian National Research Council, 70126 Bari, Italy (e-mail: leo@ba.issia.cnr.it; dorazio@ba.issia.cnr.it).

D. Looney and D. P. Mandic are with the Department of Electrical and Electronic Engineering, The Imperial College of Science, Technology and Medicine, SW7 2BT London, U.K. (e-mail: david.looney06@imperial.ac.uk; d.mandic@imperial.ac.uk).

Color versions of one or more of the figures in this paper are available online at http://ieeexplore.ieee.org.

Digital Object Identifier 10.1109/TIM.2011.2150630

Traditionally, abnormal deviations and/or anomalies are detected by trained human operators, but, unfortunately, this approach does not ensure an adequate reliability level, and at the same time, it requires prohibitive amounts of time and high costs. In addition, humans cannot detect cracks or any other irregularities in the structure components which are not visible to the naked eye.

To address the aforementioned problems, many alternative methodologies and techniques have been proposed to perform nondestructive inspection (NDT) and maintenance operations. These are based on the analysis of different signals such as ultrasonics, acoustic emissions, thermography, laser ultrasonics, X-radiography, eddy currents, shearography, and low-frequency methods [5]. In particular, in the last decade, ultrasonic techniques have shown to be very promising for NDT and the control of components in engineering systems, becoming an effective alternative to such traditional and well-studied approaches such as thermography, eddy currents, and shearography.

Most of the works in the literature describing ultrasound-based techniques for inspection and evaluation purposes concentrate on the study of data acquisition and manipulation processes in order to prove the relationship between data and structural defects or composition of the material [6]–[11]. Some of the work is based on the *a posteriori* analysis of the ultrasound data in order to (fully or partially) refer to some computational algorithm the automatic recognition of material composition, operative conditions, presence of defects, and so on. Works concerning this subject, on which this paper is focused, are less developed, and moreover, their level of inspection reliability is still inadequate, particularly for those sectors (namely transportation) where an error can have serious health and safety consequences.

The pioneering works on the *a posteriori* analysis of ultrasonic data date back to the early 1990s: they suggested that solutions to the problem of automatic ultrasonic NDT data interpretation could be found by expert systems which embody the knowledge of human interpreters [12], [13]. More effective approaches, based on advanced signal processing and artificial intelligence paradigms, have been proposed in the last decade. In [14], the authors addressed the flaw detection problem by using a radial basis function neural network, and they tried to demonstrate that a neural-based approach overcame the classical threshold-based approach for flaw detection problems. In [15], the wavelet transform was used in conjunction with an artificial neural network to distinguish the ultrasonic flaw echoes from those scattered by microstructures. A similar approach

was introduced in [16] which addressed the problem of pipe inspection by ultrasonic guided waves. The automatic detection of internal defects in composite materials with nondestructive techniques based on ultrasonic techniques was addressed also in [17]. The authors proposed a preliminary iterative normalization procedure in order to manage materials of different thickness and a two-level set of neural classifiers that segment defective areas from sound areas and determine the different defect characteristics (such as defect position and the defect type). The author's idea in [18] was, instead, to cluster the signals in the similarity space (using the Kohonen self-organizing algorithm to cluster data sets in an unsupervised manner) and then to use this result in order to distinguish between signals corresponding, respectively, to nondefects, flat defects (cracks), and volumetric defects. A high-resolution pursuit-based signal processing method was proposed in [19] for detecting flaws close to the surface of strongly scattering materials, such as steel and composites, in NDT applications. In [20], an approach to nondestructive pipeline testing using ultrasonic imaging was proposed. In [21], an evaluation of various types and configurations of neural networks developed for the purpose of assisting in accurate flaw detection in steel plates was illustrated, whereas, in [22], a neural network was trained, by using the time/space variations in a sequence of thermographic images, to extract the information that characterizes a range of internal defects in different types of composite materials.

Despite the large effort that has been put into devising efficient algorithms for this purpose, there is still a lot of work to do in order to satisfy the performance requirements of the considered application context where noise, complexity, and uncertainty play a major role. The use of multiple sensors in conjunction with advanced data fusion (the classifier operates on either the raw data or features extracted directly from the multiple sensor measurements obtained from associated databases, if appropriate) or decision fusion approaches (the decisions from the individual classifiers for different data channels are combined) [23], recently introduced in somewhat related applications (e.g., understanding and interpreting biomedical signals for healthcare), could be an effective way to pursue improved accuracies and more specific inferences [24] but, on the other hand, introduce a potentially overwhelming quantity of data that requires further investigation to reduce computational cost and required storage space [25].

In summary, it is evident that the neural paradigms are considered the best choice to classify ultrasound data in an automatic inspection system. At the same time, the most appropriate preprocessing technique is still undecided. As widely demonstrated in recent related works involving automatic pattern identification using neural paradigms [26], [27], the wavelet-based approaches appear to be the most promising, but, considering that in the considered context an error could waste time, money, and even endanger someone's life, further efforts have to be done in order to increase reliability.

The aim of this paper is to propose a new and innovative data preprocessing technique to explore the patterns embedded in the data. A methodology is first proposed to obtain a complex-valued representation for each of the ultrasound signals. By design, the complex representation highlights the presence or absence of defects in the analyzed material. This representation is then decomposed using complex/bivariate extensions of empirical mode decomposition (EMD) [28], [29] into a set of complex-valued oscillating components, known as intrinsic mode functions (IMFs). In this way, the phase information for the real and imaginary components can be defined locally [30]. This facilitates the detection of phase synchrony, that is, the temporal locking of phase information between the components, which is an established tool in brain science for performing feature extraction [31]. The existence of phase synchrony, across time and frequency, is used to characterize the degree of shared dynamics between the components of the complex representation and is consequently used to detect the possible presence of defects.

It is this methodology of converting a real-valued data source into a complex signal in order to obtain a set of synchrony features that is novel to our work. The new data representation is then applied as an input to a supervised neural classifier trained to recognize the defective areas from the nondefective ones. To demonstrate the effectiveness of the proposed approach, it has been applied to detect and classify internal defects in composite materials and, in particular, in a honeycomb structure containing different inserts placed to simulate some of the most common defective situations in composite materials.

The remainder of this paper is organized as follows: Section II describes EMD and its extensions while Section III describes the process by which phase synchrony is estimated. Section IV describes the proposed approach, and Section V describes the experimental setup and reports the results of different experiments which demonstrate the effectiveness of the proposed approach with respect to the related techniques from the literature. Finally, in Section VI, conclusions and future research directions are considered.

II. EMD and Extensions

The following sections describe EMD and bivariate EMD (BEMD).

A. EMD Algorithm

EMD [28] is a data-driven time-frequency technique which adaptively decomposes a signal, by means of a process called the sifting algorithm, into a finite set of AM/FM modulated components. These components, called "IMFs," represent the oscillation modes embedded in the data. By definition, an IMF is a function for which the number of extrema and the number of zero crossings differ by at most one, and the mean of the two envelopes associated with the local maxima and local minima is approximately zero. The EMD algorithm decomposes the signal $x(t)$ as

$$x(t) = \sum_{i=1}^{M} C_i(t) + r(t) \tag{1}$$

where $C_i(t)$, $i = 1, \ldots, M$, represents the IMFs and $r(t)$ is the residual. The first IMF is obtained as follows [28].

1) Let $\tilde{x}(t) = x(t)$.

2) Identify all local maxima and minima of $\tilde{x}(t)$.
3) Find an "envelope" $e_{\min}(t)$ [respectively, $e_{\max}(t)$] that interpolates all local minima (respectively, maxima).
4) Extract the "detail" $d(t) = \tilde{x}(t) - (1/2)(e_{\min}(t) + e_{\max}(t))$.
5) Let $\tilde{x}(t) = d(t)$, and go to step 2); repeat until $d(t)$ becomes an IMF.

Once the first IMF is obtained, the procedure is applied iteratively to the residual $r(t) = x(t) - d(t)$ to obtain all the IMFs. The extracted components satisfy the so-called mono-component criteria, and the Hilbert transform can be applied to each IMF separately. This way, it is possible to generate analytic signals, having an IMF as the real part and its Hilbert transform as the imaginary part, that is, $x + j\mathcal{H}(x)$, where $\mathcal{H}(\cdot)$ is the Hilbert transform operator. Equation (1) can therefore be augmented to its analytic form given by

$$X(t) = \sum_{i=1}^{M} a_i(t) \cdot e^{j\theta_i(t)} \tag{2}$$

where the trend $r(t)$ is purposely omitted, due to its overwhelming power and lack of oscillatory behavior. Observe that, now, from (2), the time-dependent amplitude $a_i(t)$ and phase function $\theta_i(t)$ can be extracted. By plotting the amplitude $a_i(t)$ versus time t and instantaneous frequency $f_i(t) = d\theta_i/dk$ [32], a time–frequency-amplitude representation of the entire signal is obtained, the so-called Hilbert–Huang spectrum.

B. Complex Extensions of EMD

Several extensions of EMD to the field of complex numbers have been recently developed. These include "complex EMD" [33], "rotation-invariant EMD (RIEMD)" [34], and "bivariate EMD (BEMD)" [29]. However, only RIEMD and BEMD operate directly in $\mathbb{C}$ making them suitable in practical applications [35]. In particular, BEMD facilitates enhanced local mean estimation compared to RIEMD [35] and was used in synchrony analysis.

In order to obtain a set of M complex/bivariate IMFs $\gamma_i(t)$, $i = 1, \ldots, M$, from a complex signal $z(t)$ using BEMD, the following procedure is adopted [29]:

1) Let $\tilde{z}(t) = z(t)$.
2) To obtain Q signal projections, given by $\{p_{\theta_q}\}_{q=1}^{Q}$, project the complex signal $\tilde{z}(t)$, by using a unit complex number $e^{-j\theta_q}$, in the direction of θ_q as

$$p_{\theta_q} = \Re\left\{e^{-j\theta_q}\tilde{z}(t)\right\}, \quad q = 1, \ldots, Q \tag{3}$$

   where $\Re\{\cdot\}$ denotes the real part of a complex number and $\theta_q = 2q\pi/Q$.
3) Find the locations $\{t_j^q\}_{q=1}^{Q}$ corresponding to the maxima of $\{p_{\theta_q}\}_{q=1}^{Q}$.
4) Interpolate (using spline interpolation) between the maxima points $[t_j^q,\ \tilde{z}(t_j^q)]$ to obtain the envelope curves $\{e_{\theta_q}\}_{q=1}^{Q}$.
5) Obtain the mean of all the envelope curves $m(t)$ and subtract from the input signal, that is, $d(t) = \tilde{z}(t) - m(t)$. Let $\tilde{z}(t) = d(t)$, and go to step 2); repeat until $d(t)$ becomes an IMF.

Similarly to real-valued EMD, once the first IMF is obtained $\gamma_1(t)$, the procedure is applied iteratively to the residual $r(t) = z(t) - d(t)$ to obtain all the IMFs.

Once the IMFs have been obtained, the real and imaginary components can be treated as two sets of IMFs: $\Re\{\gamma_i(t)\}$ and $\Im\{\gamma_i(t)\}$. The instantaneous amplitudes, namely, $\Re\{a_i(t)\}$ and $\Im\{a_i(t)\}$, and phases, namely, $\Re\{\theta_i(t)\}$ and $\Im\{\theta_i(t)\}$, for each set of IMFs can then be determined.

Consider a complex signal $z = x_1 + jx_2$. The real and imaginary parts of z are given, respectively, in the first panels of Fig. 1(a) and (b). The real part of the decomposition obtained using BEMD for z is shown in the subsequent panels of Fig. 1(a), and the imaginary part is shown in the subsequent panels of Fig. 1(b). Note that, for convenience, not all the high-frequency IMFs have been displayed. For example, the second panel of Fig. 1(a) shows the summation of the first six real-valued IMFs $\sum_{i=1}^{6} \Re\{\gamma_i\}$. Observe how the BEMD operation presents a data-driven framework to compare the temporal scales of z.

III. Phase Synchrony

Phase synchrony between two signals is defined as the temporal locking of phase information. That is, for a given frequency, phase synchrony exists if the phase difference remains constant over a period of time. It is a popular tool in brain science for robustly modeling any shared dynamics that exist between the sources. To measure the phase synchrony between x_1 and x_2, BEMD is first applied to the complex signal $x_1 + jx_2$. The instantaneous phase difference between the real and imaginary parts of each IMF component is given by $\psi_i(t)$. The degree of phase synchrony between x_1 and x_2 is given by [30]

$$\phi_i(t) = \frac{H_{\max} - H}{H_{\max}} \tag{4}$$

where $H = -\sum_{n=1}^{N} p_n \ln p_n$ represents the Shannon entropy of the distribution of $\psi_i(t - (W/2) : t + (W/2))$ defined by a window of length W, N is the number of bins, and p_n is the probability of $\psi_i(t - (W/2) : t + (W/2))$ within the nth bin [36]. The maximum entropy $H_{\max}$ is given by

$$H_{\max} = 0.626 + 0.4\ln(W - 1). \tag{5}$$

The value of ϕ is between zero and one, with one indicating perfect synchrony and zero a nonsynchronous state. An additional step can be incorporated to model simultaneously for component relevance

$$\phi_i(t) = \begin{cases} 0, & \text{if } \Re\{a_i(t)\} < \epsilon \\ 0, & \text{if } \Im\{a_i(t)\} < \epsilon \end{cases} \tag{6}$$

where ϵ is an appropriate threshold. Once the phase synchrony information has been estimated, it can be conveniently represented by the matrix $\rho(f, t)$, which denotes the phase synchrony at index t and frequency f.

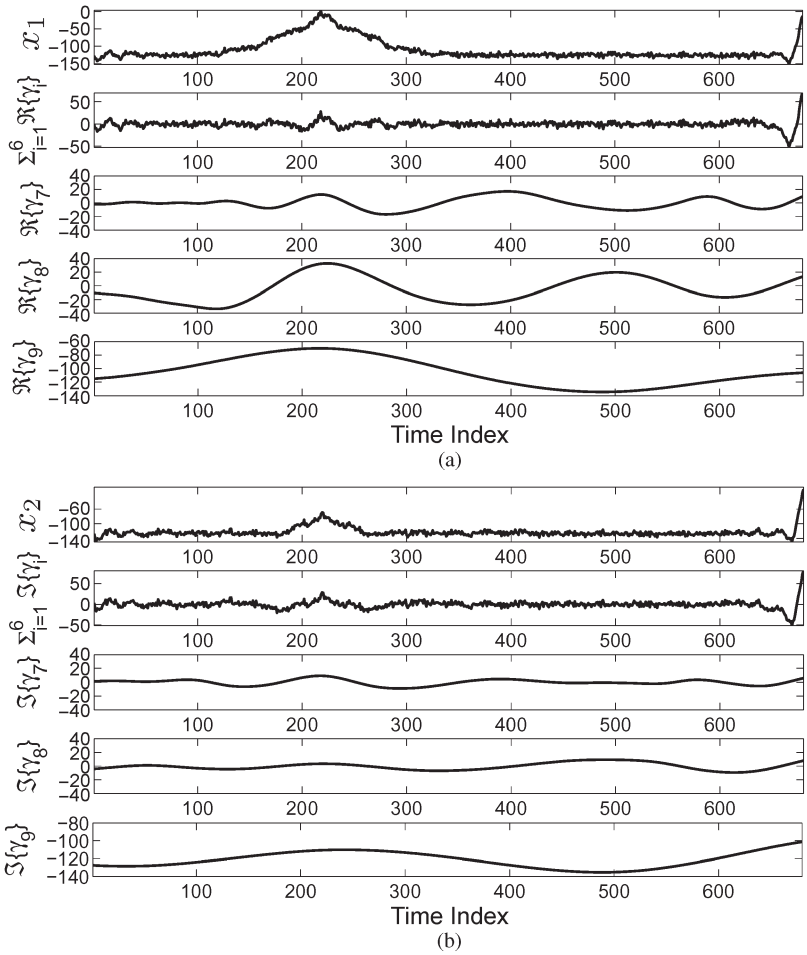

Fig. 1. Decomposition of $z = x_1 + jx_2$, shown in the top panels of (a) and (b), into a set of complex IMFs γ_i using BEMD. (a) Real component. (b) Imaginary component.

IV. Proposed Approach

Ultrasonic inspection uses sound signals at frequencies beyond human hearing (more than 20 kHz) to estimate some properties of the irradiated material by analyzing either the reflected (reflection working modality) or transmitted (transmission working modality) signals. A typical ultrasonic inspection system consists of several functional units: pulser, receiver, transducer, and display devices. A pulser is an electronic device that can produce a high-voltage electrical pulse. Driven by the pulser, the transducer generates a high-frequency ultrasonic wave which propagates through the material. In the transmission modality, the receiver is placed on the opposite side of the material from the pulser, whereas, in the reflection modality, the pulser and the receiver are placed on the same side of the material.[1]

Ultrasonic data can be collected and displayed in a number of different formats. The three most common formats are known in the NDT community as A-scan, B-scan, and C-scan presentations. Each presentation mode provides a different way of looking at and evaluating the region of material being inspected. In this paper, the analysis of ultrasonic data acquired from the reflection working modality and A-scan representation is reported. This means that, for each point of the inspected material, we have a continuous signal that represents the amount of received ultrasonic energy as a function of time.

The temporal evolution of the ultrasound signal $x(t)$ is the input to the core of the proposed approach that consists of two main steps: the preprocessing of the data in order to emphasize the characteristics of the signals belonging to the same class, and the following neural classification. Fig. 2 shows the different procedures involved in the proposed approach. In the preprocessing step, a methodology is first proposed to extend each real-valued ultrasonic signal $x_{u,v}(t)$, where (u, v) denotes a point in the material, to the complex domain $Z_{u,v}(t)$.

Consider first an ultrasonic signal for an area of the material that is defect free; see Fig. 3(a). Observe that there are large extrema at the beginning and at the end. These changes in ultrasound energy are caused by the transmitted signals being reflected by the boundaries of the material. These boundary extrema are referred to as toolside and bagside peaks, respectively. The ultrasonic signal for an area of material that contains defects is, instead, given in Fig. 4(a). Note that, in addition to the boundary extrema, the signal contains extrema at other time locations caused by defective components. A defect-free area of material is therefore characterized by a data set which

[1]Inspection devices may or may not be in contact with the material. In the former case, a liquid or a paste (couplant) is used to facilitate the transmission of ultrasonic vibrations from the transducer to the test surface. In noncontact ultrasound, ambient air is instead the only acoustic coupling medium.

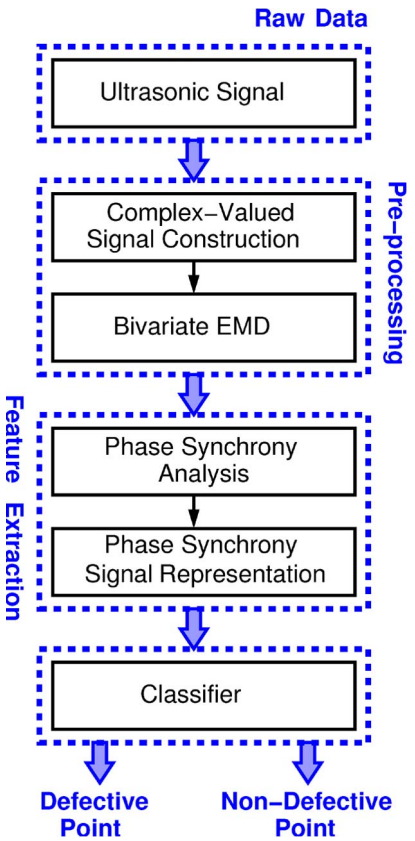

Fig. 2. Schematic representation of the different procedures involved in the proposed approach.

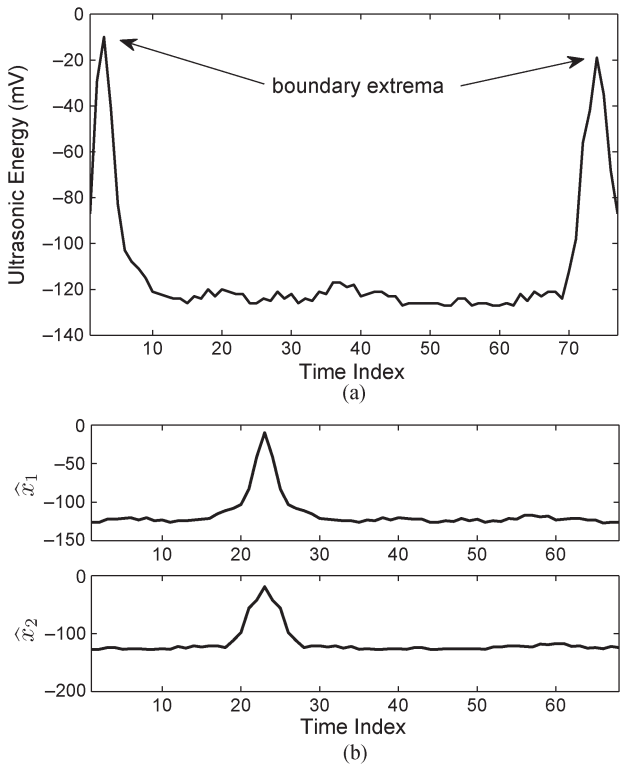

Fig. 3. (a) Example of a nondefective ultrasonic signal and (b) its complex extension.

is symmetrical about its center and contains boundary extrema only. Thus, it is proposed to divide each data set about its center

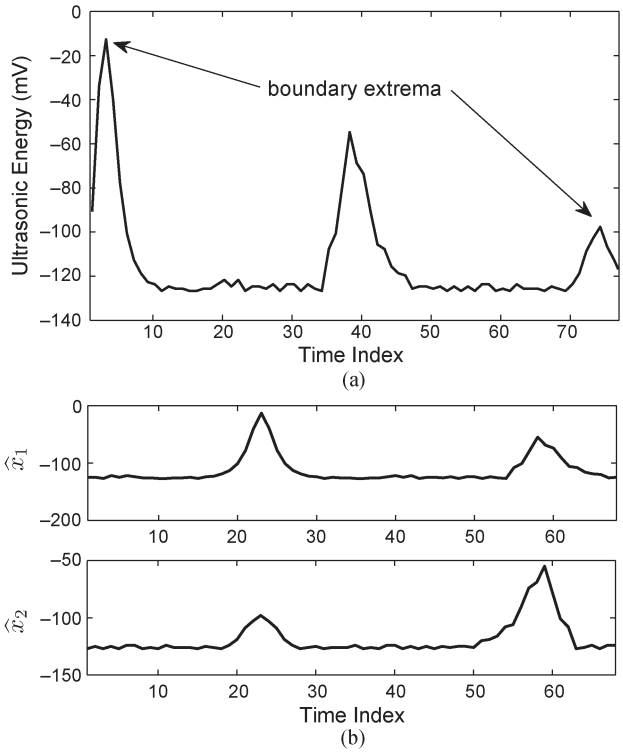

Fig. 4. (a) Example of a defective ultrasonic signal and (b) its complex extension.

$x(T/2)$, thus producing two segments, namely, x_1 and x_2, by

$$\begin{aligned} &x_1\left(1,2,\ldots,\frac{T}{2},\ldots,\frac{T}{2}+K_R\right) \\ &\quad = x\left(1,2,\ldots,\frac{T}{2},\ldots,\frac{T}{2}+K_R\right) \\ &x_2\left(1,2,\ldots,\frac{T}{2},\ldots,\frac{T}{2}+K_R\right) \\ &\quad = x\left(T,T-1,\ldots,\frac{T}{2},\ldots,\frac{T}{2}-K_R\right). \end{aligned} \tag{7}$$

Note that each segment is additionally extended by K_R points at the right-sided edge $(t = T/2)$. These segments are then extended at the left-sided edge by K_L points. These segments are denoted by $\widehat{x}_1$ and $\widehat{x}_2$ and are dependent on the position of the toolside peak and bagside peak, respectively. If, for example, the boundary extremum relevant to $x_1(t)$, that is, the toolside peak, occurs at $t = e_1$, then $\widehat{x}_1(t)$ is given by

$$\begin{aligned} \widehat{x}_1\left(e_1,\ldots,\frac{T}{2}+K_R\right) &= x_1\left(e_1,\ldots,\frac{T}{2}+K_R\right) \\ \widehat{x}_1(e_1-1,\ldots,e_1-K_L) &= x_1(e_1+1,\ldots,e_1+K_L) \end{aligned} \tag{8}$$

where $\widehat{x}_2(t)$ is constructed in a similar fashion around the bagside peak. The extended components for the ultrasonic signals shown in Figs. 3(a) and 4(a), are shown, respectively, in Figs. 3(b) and 4(b). Thus, the complex extension of the real-valued ultrasound signal, for point (u, v), is given by $Z_{u,v}(t) = \widehat{x}_1(t) + j\widehat{x}_2(t)$.

The signal $Z_{u,v}(t)$ is decomposed into a set of complex oscillation modes (IMFs) $\gamma_i(z)$, where $i = 1, \ldots, M$, by applying

a complex extension of EMD, i.e., BEMD [29]. The real and imaginary parts of the decomposition $\Re\{\gamma_i(t)\}$ and $\Im\{\gamma_i(t)\}$ denote the IMFs for $\widehat{x}_1(t)$ and $\widehat{x}_2(t)$, respectively. By construction, the phase information for each IMF is well defined at each instant t and facilitates a highly localized comparison between the phase information of $\widehat{x}_1(t)$ and $\widehat{x}_2(t)$ [30]. The degree of phase synchrony, which is the temporal locking of phase information between $\Re\{\gamma_i(t)\}$ and $\Im\{\gamma_i(t)\}$, is then determined to characterize the dynamics of $Z_{u,v}(t)$, that is the symmetry of the original ultrasound signal about its center as well as the location of its extrema. The information is represented by a matrix $\rho_{u,v}(f,t)$ which denotes the synchrony at index t and frequency f.

In the analysis, two additional preprocessing steps were performed on the complex data representation, $Z_{u,v}(t)$, in order to facilitate more robust synchrony estimation. Synchrony analysis involves the calculation of entropy for phase distributions which requires long data lengths so $Z_{u,v}(t)$ was initially upsampled. Furthermore, a noise-assisted EMD facilitates a more natural separation of scale components [37]. For this reason, white Gaussian noise was added to the real and imaginary components before applying BEMD, and $\rho_{u,v}(f,t)$ was obtained by averaging the synchrony results over several realizations of noise.

The synchrony matrix for each ultrasound signal $\rho_{u,v}(f,t)$ is then vectorised and downsampled. Principal component analysis (PCA) is then applied to reduce dimensionality giving a feature vector $Y_{u,v} = [y_1, y_2, \ldots, y_N]$ for each ultrasound signal. The M most informative components are finally given as the input to a ***neural classifier*** trained with a *back propagation algorithm* to distinguish defective from nondefective areas.

V. Experimental Setup and Results

To illustrate the effectiveness of the proposed approach, a set of ultrasound measurements on a composite material has been considered. The material has a honeycomb structure with Nomex Core and 128 ply thicknesses (each ply has a thickness of 0.19 mm). Ultrasonic data was obtained by an ultrasonic reflection technique that uses a single transducer serving as transmitter and receiver (5 MHz).

The collected data are relative to defective and nondefective areas: defective areas contain artificial defects introduced during the manufacturing process and are composed of the following materials: brass foil (0.02 ± 0.01 mm thick), pressure sensitive tape,[2] and dry peel ply (0.12 mm thick). In particular, brass inserts, dry peel ply, and adhesive tape were introduced to represent voids and delamination, inclusions by means of reflection techniques, and inclusions by means of transmission techniques, respectively. In the following, [A] stands for tape, [F] stands for peel ply, and [B] stands for brass. The typical insert locations are the following:

1) one and two plies from toolside surface for brass and pressure sensitive Tape and 1016 mm from toolside surface for peel ply (**Top**);
2) midpart thickness (**Mid**);
3) one and two plies from bagside surface for brass and pressure sensitive tape and 1016 mm from bagside surface for peel ply (**Bottom**).

Each $x_{(u,v)}(t)$, which is the ultrasound signal corresponding to point (u,v), contains 77 temporal samples. This signal was converted into a complex signal $Z_{(u,v)}(t)$, and synchrony analysis was performed on the IMFs obtained by applying BEMD to the upsampled signal. Because of the initial upsampling, only low-frequency synchrony information was considered in the analysis. Each synchrony matrix $\rho_{(u,v)}$ was then vectorised and downsampled obtaining a 1198-long feature vector. This is the input of the classification step involving PCA data reduction and neural classification of defective and nondefective points.

First of all, the experimental data set consisting of 2620 ultrasound signals was built. Specifically, the data set was composed of 1920 signals acquired for the three different types of defect (640 signals for each defect type: [A], [B], and [F]) and 700 signals obtained from areas which did not contain any defects. For each defect type, the points in the data set were equally relative to the defects placed at midthickness level, at the top, and at the bottom of the inspected material.

The aim of the preliminary experimental phase was to determine the values of some important parameters of the proposed framework. The number of required principal components (PCs) was first considered. This is a crucial step considering that underestimation of this number would discard valuable information, whereas overestimation could result in a large number of spurious components carrying useless information that could compromise further steps in data classification. A popular ad hoc rule is to plot the eigenvalues in decreasing order (scree plot) and search for a peak which denotes that the signal eigenvalues are on the left side and the noise eigenvalues are on the right. Another approach is to compute the cumulative percentage of the total variation explained by the PCs and retain the number of PCs that represents 70% or 80% of the total variation [38]. The choice of the number of components to retain could be also seen as a problem of model selection. This probabilistic reformulation of PCA permits many extensions [39]. Two interesting approaches were formulated in [40] and [41]: the authors developed a model selection criterion for estimating the true dimension of the observed data set (or the number of PCs to retain) where "true dimension" denoted the sufficient dimension to fully describe the information available.

In Fig. 5, the variance and the cumulative variance of the first 200 PCs computed from the considered data set are plotted. In Fig. 6, a probabilistic analysis of the PCs is reported. The dashed curve shows the likelihood relative to different data dimensionality computed by the method proposed in [40], which makes use of Bayesian model selection, and for this reason, it is referred to as the Bayesian information criterion. In a similar way, the solid curve indicates the likelihood computed by the method proposed in [41] and is referred to as Laplace (it makes use of the Laplace's method to get model parameter estimation). Statistical and probabilistic information in Figs. 5

[2]American Biltrite 6782, Tape Product Division, American Biltrite, Inc., 105 Whittendale, Moorestown, NJ, 08057

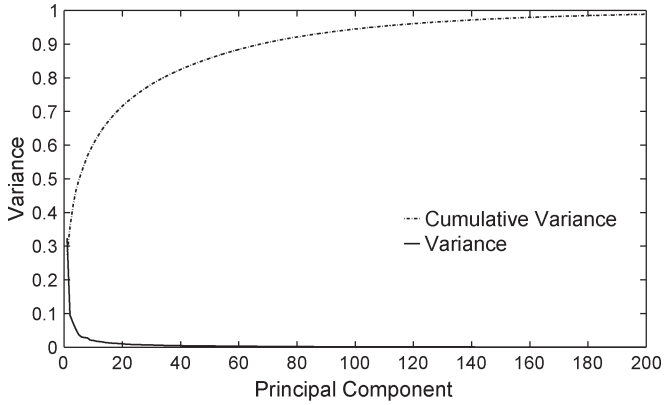

Fig. 5. Variance and cumulative variance of the first 200 PCs.

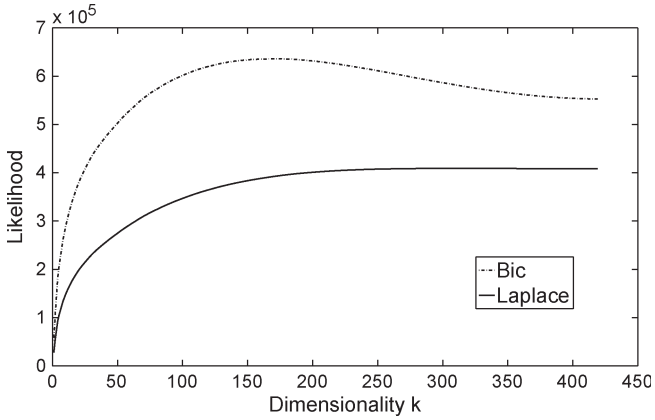

Fig. 6. Probabilistic analysis of the PCs.

and 6 indicate that the optimal number of PCs that should be retained is 70.

Once the number of significant PCs was fixed, the feature vector $Y_{(u,v)} = [y_1, y_2, \ldots, y_{70}]$ for each ultrasound signal was calculated. The next step was to select the most appropriate neural architecture for the considered problem. A three-layer feedforward network, with *tansig* activation functions in the hidden layer and *linear* activation functions in the output layer, is often used in the literature. Considering that the problem requires binary classification and that there exists a sufficient amount of data examples for each of the two classes, the back propagation algorithm was used to train the neural network. The number of neurons of the input layer was set to the number of input variables (i.e., 70), and the number of neurons in the output layer was one. The network was trained such that the output value 1 denoted a defective signal and the value -1 denoted a nondefective signal.

The network size has a strong influence on the network performance: setting too few hidden units causes high training errors and high generalization errors due to underfitting, while too many hidden units results in low training errors but still high generalization errors due to overfitting. Despite this, there is no straightforward way to obtain the correct number of hidden layer neurons for the considered task. Several researchers have proposed some ad hoc solutions to this problem. However, such rules are not applicable in most circumstances as they do not consider the training set size (number of training pairs), the complexity of the data set to be learnt, etc. It is argued that

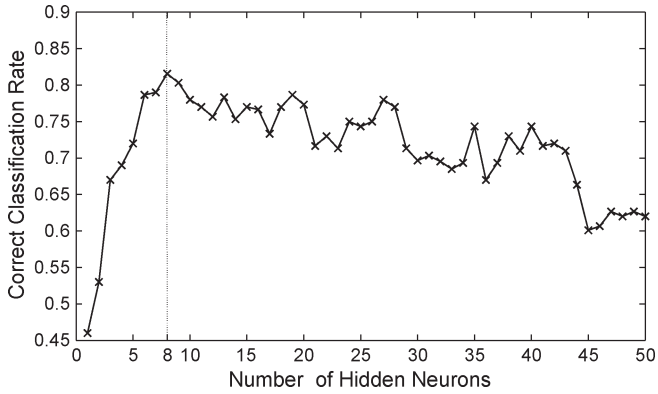

Fig. 7. Overall classification error obtained with different numbers of neurons in the hidden layer of the network architectures.

the optimal number of hidden units depends on the numbers of input and output units, the number of training cases, the amount of noise in the targets, the complexity of the function or classification to be learned, the architecture, the type of hidden unit activation function, the training algorithm, etc. Thus, in the experiments, different neural architectures (with the number of hidden neurons ranging from 1 to 50) were considered, and their classification performances were evaluated.

The experimental phase made use of a training set consisting of 500 ultrasonic signals: 300 signals were relative to defective points, whereas the remaining 200 were relative to nondefective points. The 300 defective training points belonged to the three defect types (100 for [A], 100 for [B], and 100 for [F]), and for each type, 40 of them were relative to defects placed at the top, 40 to defects placed at the bottom, and 20 to defects placed in the middle part of the material.

The ability to classify the remaining 2120 signals of the data set as defective or nondefective was then evaluated in *the first experimental phase*. In Fig. 7, the correct classification rate for each neural architecture is shown. It is possible to observe that the best rate (84.15%) was obtained with eight neurons in the hidden layer. This demonstrated that, while a lower number of neurons limited the knowledge of the input data (underfitting), a higher number of neurons made it difficult for the classifier to generalize that knowledge (overfitting).

In Table I, classification performance using the optimal neural architecture is shown. The left column states the type and the thickness level placement of the testing signals. For example, [A]-m refers to signals extracted from [A]-type defective areas placed at the midthickness level. In the same column, the signals extracted from areas which did not contain any defects are referred as "ND." The middle and right columns report the classification results (in terms of defective/nondefective signals) obtained by the proposed approach.

Although the correct defect identification rate is high, it can be deduced that the performance of the proposed methodology depends on both the following:

1) the defect type;
2) the defect location in the inspected material.

Table I illustrates that defective areas at the midthickness level are always better classified than those located either at the top or at the bottom. The defect location is one of the most

TABLE I
CLASSIFICATION PERFORMANCES WITH THE OPTIMAL NEURAL NETWORK ARCHITECTURE

	Defective Points	Non-Defective Points
[A]-m	**179/180 (99.45%)**	1/180 (0.55%)
[B]-m	**174/180 (96.66%)**	6/180 (3.33%)
[F]-m	**171/180 (95.00%)**	9/180 (5.00%)
[A]-t	**166/180 (92.22%)**	14/180 (7.77%)
[B]-t	**154/180 (85.55%)**	26/180 (14.44%)
[F]-t	**150/180 (83.33%)**	30/180 (16.66%)
[A]-b	**159/180 (88.33%)**	21/180 (11.66%)
[B]-b	**157/180 (87.22%)**	23/180 (12.77%)
[F]-b	**151/180 (83.88%)**	29/180 (16.11%)
ND	179/500 (35.80%)	**321/500 (64.20%)**
TOTAL	Correct *1782/2120 (84.00%)*	Incorrect *336/2120 (16.00%)*

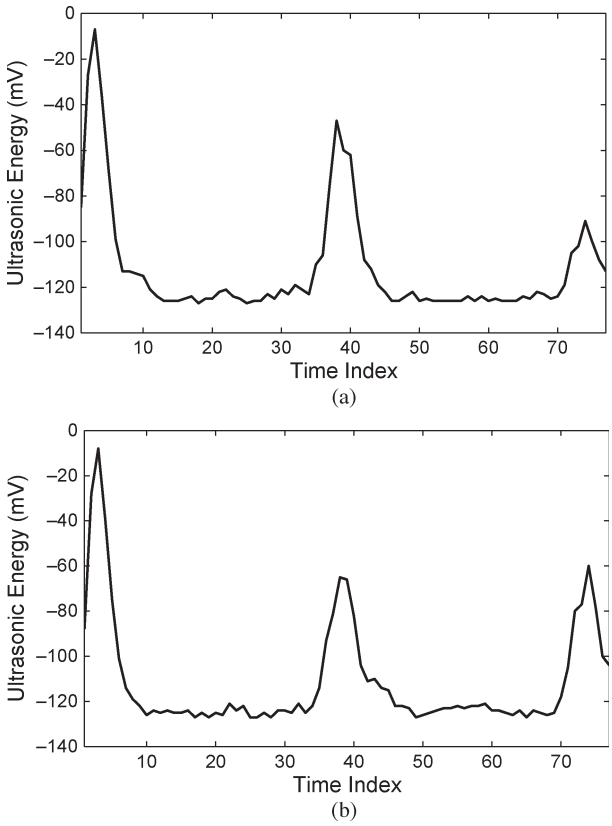

Fig. 8. Two signals pointing out the different acoustic reflection coefficient for two different defect types. (a) Example of acoustic reflection for an [A]-type defect. (b) Example of acoustic reflection for an [F]-type defect.

important factors in ultrasound inspection. The defects placed either at the top or at the bottom of the inspecting structure are, in general, the most difficult to detect since their echo is mixed with the toolside or the bagside echo. However, defective areas in the midpart of the material thickness produce a distinct peak in the signal trend that is straightforward to identify [compare Figs. 3(a) and 4(a)].

From Table I, it is clear that the defect type also affects the classification rate. Each defect type has a different acoustic reflection coefficient. The larger this acoustic coefficient, the more prominent it will be in the ultrasound data and the more straightforward the defect is to detect. In particular, it is observed that [A]-type defective points were better identified than [B]. The most poorly identified was the [F]-type

TABLE II
CORRECT DEFECT IDENTIFICATION RATE FOR THE THREE COMPARED APPROACHES

	BEMD	Direct input	Wavelet
[A]-m	179/180 (99.45%)	165/180 (91.66%)	170/180 (94.44%)
[B]-m	174/180 (96.66%)	155/180 (86.11%)	160/180 (88.88%)
[F]-m	171/180 (95.00%)	148/180 (82.22%)	158/180 (87.77%)
[A]-t	166/180 (92.22%)	116/180 (64.44%)	158/180 (87.77%)
[B]-t	154/180 (85.55%)	38/180 (21.11%)	92/180 (51.11%)
[F]-t	150/180 (83.33%)	74/180 (41.11%)	139/180 (77.22%)
[A]-b	159/180 (88.33%)	111/180 (61.66%)	149/180 (82.77%)
[B]-b	157/180 (87.22%)	68/180 (37.77%)	144/180 (80.00%)
[F]-b	151/180 (83.88%)	100/180 (55.55%)	114/180 (63.33%)
SUB TOTAL	***1464/1620 (90.37%)***	975/1620 (60.18%)	1284/1620 (79.25%)
ND	321/500 (64.20%)	***482/500 (96.40%)***	459/500 (91.80%)
TOTAL	*1782/2120 (84.00%)*	*1447/2120 (68.25%)*	*1743/2120 (82.21%)*

defects. In Fig. 8, the different acoustic reflection behavior for [A]-type [Fig. 8(a)] and [F]-type [Fig. 8(b)] defects is shown. The [A]-type defect reflects much more acoustic energy than the [F]-type as is illustrated by both the higher amplitude of the central echo and the lower amplitude of the bagside echo.

The second experimental phase compared the proposed approach with the methods that are among the most effective in automatic defect identification. In particular, two other approaches were considered. For the first method, the ultrasonic signals were classified by a neural network without any preprocessing (specifically, the 77 available samples for each point were given as input to the net after the normalization in the range $[-1,1]$). For the second method, classical preprocessing based on the wavelet decomposition was applied to the ultrasonic signal, and selected coefficients were supplied to the neural classifier.[3] The same neural architecture as before was used to classify the features obtained for both methods. The optimal number of hidden neurons was experimentally found to be 30 for the wavelet-based approach and 15 for the direct approach with no preprocessing.

Table II compares results for the three approaches, obtained using the same data set as before. On the one hand, the proposed BEMD-based approach gave the best defect identification rate (for all considered defect types and defect locations), but, on the other hand, it also generated a larger number of false positives for nondefective points.

In particular, it is evident that BEMD preprocessing can accurately detect certain defective points, placed at the top and at the bottom of the considered material, which are not detectable

[3]The DB3 family was used, and the decomposition was carried out until level 3. The resulting 92 coefficients were then used to represent the ultrasound signal.

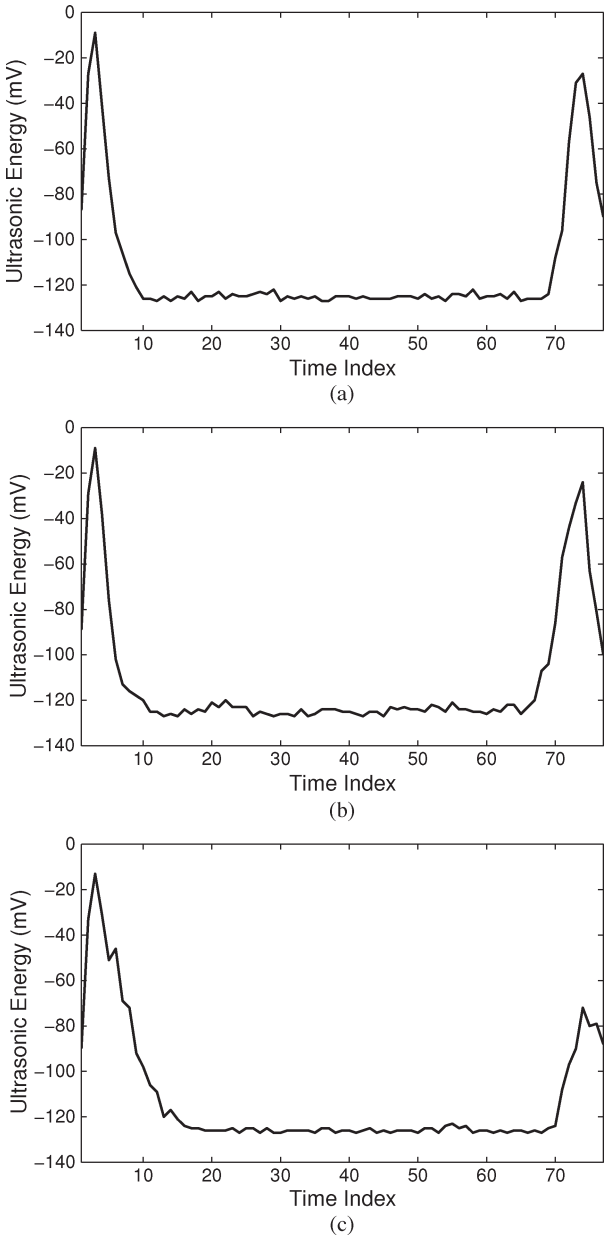

Fig. 9. Different echoes in the case of (a) a nondefective ultrasonic signal and (b)–(c) two [B]-type ultrasonic defective signals relative to defect areas placed at different location into the inspecting composite material. (a) Nondefective ultrasonic signal. (b) Ultrasonic signal relative to a defect placed two plies from toolside surface. (c) Ultrasonic signal relative to a defect placed two plies from bagside surface.

using direct-input and wavelet-based approaches. In Fig. 9, we report a nondefective ultrasonic signal [Fig. 9(a)] together with two [B]-type defective signals obtained from two areas placed two plies from the toolside surface [Fig. 9(b)] and two plies from the bagside surface [Fig. 9(c)]. The similarity of the three signals is quite evident and causes standard preprocessing techniques to fail. The proposed complex-valued representation of the ultrasonic signals highlights the small differences that can be found in the toolside and bagside peaks, and the phase synchrony analysis detects the presence of defects. Using the BEMD-based approach, only a very small percentage of defective points was missed. This performance is useful in the considered inspection context (particularly, for transportation purposes) where it is important to detect all the defective areas even at the cost of increasing the number of false positives.

The benefits of the proposed approach are further illustrated in *the third experimental phase* in which the neural architectures trained with the three different approaches were used to fully inspect a small part of the considered honeycomb structure with Nomex Core. The inspected part contains different defective insertions as shown in Fig. 10(a). Fig. 10(b)–(d) show the inspection results obtained using the direct-input, wavelet, and BEMD approaches, respectively.

Clearly, the BEMD-based approach can more accurately detect all defective areas, but it also results in a higher number of false positives. Considering that these false detections are isolated and do not form connected regions having a considerable area value, the elimination of these points is straightforward if some *a priori* knowledge about the minimum expected size of the defective areas is available. For example, in Fig. 11(a)–(c), the inspection results, after a filtering process based on the connectivity analysis of the detected defective regions and a selection criterion based on removing the regions having an area less than 20 pixels, are shown. Observe that the direct input approach completely missed three (placed on the top and on the bottom of the materials) of the nine defective insertions [see Fig. 11(a)]. Wavelet preprocessing was able to detect two of the missed insertions but still missed the [B]-type insertion placed at the top of the material [see Fig. 11(b)]. The BEMD preprocessing facilitated an increase in the percentage of detected defective points such that all the defective areas were identified [see Fig. 11(c)].

The proposed method is significantly more computationally complex than the other considered approaches.[4] However, the aim of this paper is to facilitate highly accurate analysis at the expense of computation cost. It would be possible to reduce the complexity of the EMD operation using linear envelope interpolation or adjusting stopping parameters, but this is outside the scope of this paper.

VI. Conclusion

The aim of this paper is to propose a new and innovative data preprocessing technique that converts real-valued ultrasonic signals into complex-valued signals, making them suitable to apply phase synchrony analysis using complex/bivariate extensions of EMD, a data-driven algorithm for detecting temporal scales in nonlinear and nonstationary data. It has been illustrated experimentally that the proposed preprocessing approach is suitable for detecting defective components in composite materials. Obtaining the complex-valued representation, a defect-free component is characterized by a unique similarity between the real and imaginary parts at a given time and frequency. Thus, the application of BEMD facilitates a highly localized time–frequency analysis of the complex representation, and the subsequent calculation of phase synchrony can be used to

[4]As a data-driven operation, EMD does not have a rigorous mathematical derivation, meaning that, for example, the number of decompositions cannot be controlled directly and makes accurate analysis of the computation cost difficult.

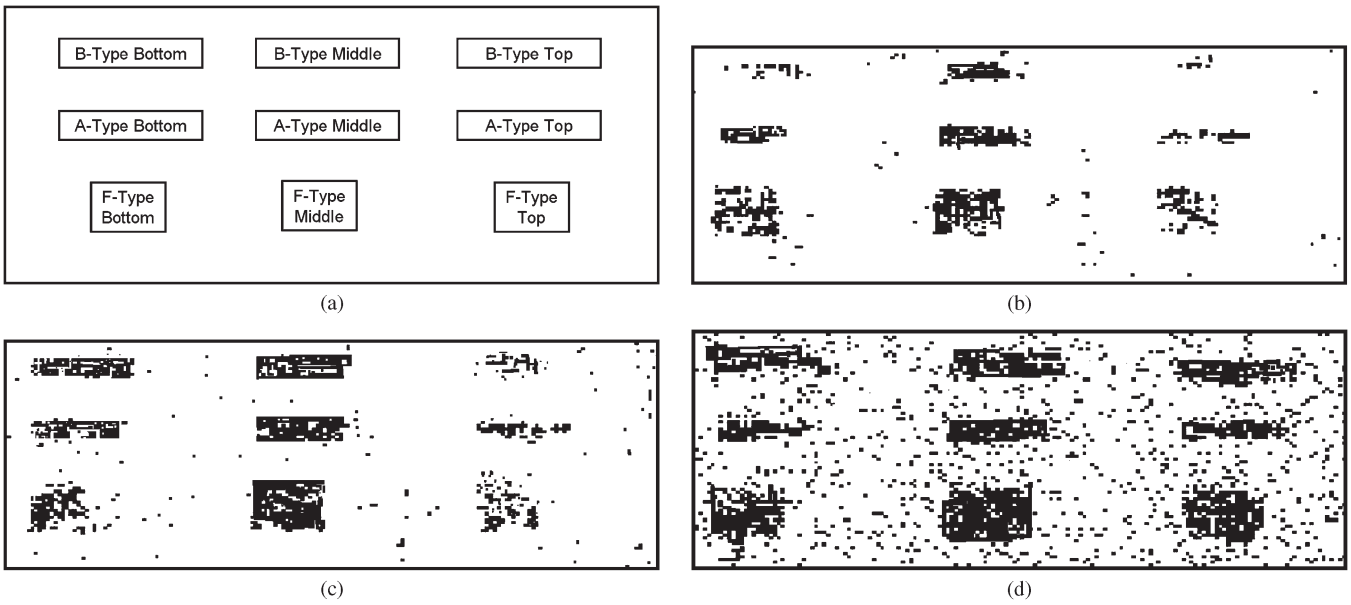

Fig. 10. Results of the inspection of (a) a honeycomb structure by using the three methods (b), (c), and (d). (a) Layout of the defective regions. (b) Inspection results obtained using the direct input. (c) Inspection results obtained using the wavelet preprocessing. (d) Inspection results obtained using BEMD preprocessing.

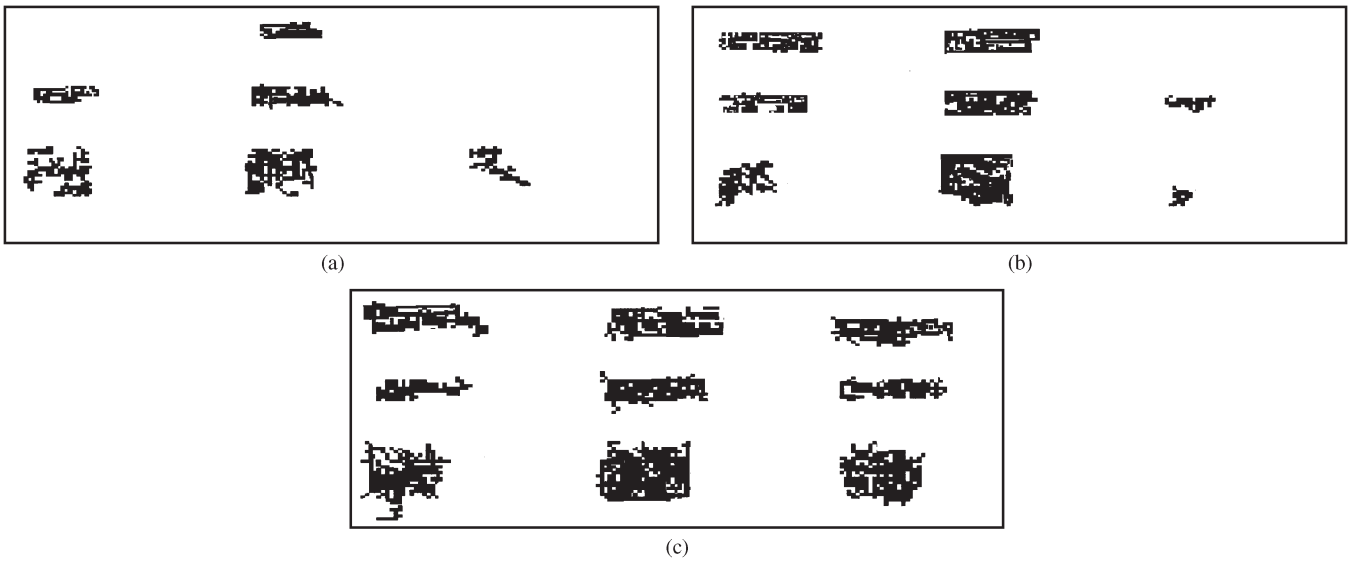

Fig. 11. Effect of a filtering process based on the connectivity analysis of the detected defective regions using a selection criterion based on the removal of points with a surrounding area value of less than 20 pixels. (a) Inspection results obtained using the direct input and a further area-based region filtering. (b) Inspection results obtained using wavelet preprocessing and a further area-based region filtering. (c) Inspection results obtained using BEMD preprocessing and a further area-based region filtering.

quantify the degree of similarity between the real and imaginary parts.

Different experiments were carried out to compare the proposed preprocessing methodology with the most common and effective preprocessing techniques found in the literature. The results have demonstrated that the BEMD-based preprocessing approach performs better in terms of defect detections and allows the recognition of defective areas at difficult-to-detect locations such as near the top or the bottom of the material, scenarios which can cause standard approaches to fail.

Future work will focus on investigating the defect-identification capability of the proposed BEMD-based approach. This will be achieved by extending the analysis to material with different thicknesses and different defective insertions. In the future, we will also investigate the possibility of using an unsupervised-learning approach in order to reduce human intervention.

REFERENCES

[1] A. Papadimitropoulos, G. A. Rovithakis, and T. Parisini, "Fault detection in mechanical systems with friction phenomena: An online neural approximation approach," *IEEE Trans. Neural Netw.*, vol. 18, no. 4, pp. 1067–1082, Jul. 2007.

[2] G. Simone and F. C. Morabito, "RBFNN-based hole identification system in conducting plates," *IEEE Trans. Neural Netw.*, vol. 12, no. 6, pp. 1445–1454, Nov. 2001.

[3] D. Mery and D. Filbert, "Automated flaw detection in aluminum castings based on the tracking of potential defects in a radioscopic image sequence," *IEEE Trans. Robot. Autom.*, vol. 18, no. 6, pp. 890–901, Dec. 2002.

[4] H. A. Talebi, K. Khorasani, and S. Tafazoli, "A recurrent neural-network-based sensor and actuator fault detection and isolation for nonlinear

systems with application to the satellite's attitude control subsystem," *IEEE Trans. Neural Netw.*, vol. 20, no. 1, pp. 45–60, Jan. 2009.
[5] C. Boller, F.-K. Chang, and Y. Fujino, *Encyclopedia of Structural Health Monitoring*. Hoboken, NJ: Wiley, 2009.
[6] S. Wagle and H. Katoa, "Ultrasonic wave intensity reflected from fretting fatigue cracks at bolt joints of aluminum alloy plates," *NDT & E Int.*, vol. 42, no. 8, pp. 690–695, Dec. 2009.
[7] A. A. Shah, Y. Ribakov, and S. Hirose, "Nondestructive evaluation of damaged concrete using nonlinear ultrasonics," *Mater. Des.*, vol. 30, no. 3, pp. 775–782, Mar. 2009.
[8] S. K. Nath, K. Balasubramaniam, C. V. Krishnamurthy, and B. H. Narayana, "An ultrasonic time of flight diffraction technique for characterization of surface-breaking inclined cracks," *Mater. Eval.*, vol. 67, no. 2, pp. 141–148, 2009.
[9] R. Y. Vun, K. Hoover, J. Janowiak, and M. Bhardwaj, "Calibration of non-contact ultrasound as an online sensor for wood characterization: Effects of temperature, moisture, and scanning direction," *Appl. Phys. A, Mater. Sci. Process.*, vol. 90, no. 1, pp. 191–196, Jan. 2008.
[10] R. S. Edwards, S. Dixon, and X. Jian, "Characterisation of defects in the railhead using ultrasonic surface waves," *NDT & E Int.*, vol. 39, no. 6, pp. 468–475, Sep. 2006.
[11] R. Raišutis, E. Jasiuniene, R. Šliteris, and A. Vladišauskas, "The review of non-destructive testing techniques suitable for inspection of the wind turbine blades," *Ultragarsas (Ultrasound)*, vol. 63, no. 1, pp. 26–30, 2008.
[12] A. McNab and I. Dunlop, "A review of artificial intelligence applied to ultrasonic defect evaluation," *Insight*, vol. 37, no. 1, pp. 11–16, 1995.
[13] A. A. Hopgood, N. Woodcock, N. J. Hallani, and P. Picton, "Interpreting ultrasonic images using rules, algorithms and neural networks," *Eur. J. Nondestruct. Test.*, vol. 2, no. 4, pp. 135–149, 1993.
[14] R. Gil Pita, R. Vicen, M. Rosa, M. P. Jarabo, P. Vera, and J. Curpian, "Ultrasonic flaw detection using radial basis function networks (RBFNs)," *Ultrasonics*, vol. 42, no. 1–9, pp. 361–365, Apr. 2004.
[15] F. Bettayeb, T. Rachedi, and H. Benbartaoui, "An improved automated ultrasonic NDE system by wavelet and neuron networks," *Ultrasonics*, vol. 42, no. 1–9, pp. 853–858, Apr. 2004.
[16] P. Rizzo, I. Bartoli, A. Marzani, and F. Lanza di Scalea, "Defect classification in pipes by neural networks using multiple guided ultrasonic wave features," *ASME J. Pressure Vessel Technol.*, vol. 127, no. 3, pp. 294–303, Aug. 2005.
[17] T. D'Orazio, M. Leo, A. Distante, C. Guaragnella, V. Pianese, and G. Cavaccini, "Automatic ultrasonic inspection for internal defect detection in composite materials," *NDT & E Int.*, vol. 41, no. 2, pp. 145–154, Mar. 2008.
[18] T. M. Meksen, B. Boudraa, and M. Boudraa, "Defects clustering using Kohonen networks during ultrasonic inspection," *IAENG Int. J. Comput. Sci.*, vol. 36, no. 3, pp. 225–228, 2009.
[19] N. Ruiz-Reyes, P. Vera-Candeas, J. Curpian-Alonso, J. C. Cuevas-Martinez, and J. L. Blanco-Claraco, "High-resolution pursuit for detecting flaw echoes close to the material surface in ultrasonic," *NDT & E Int.*, vol. 39, no. 6, pp. 487–492, Sep. 2006.
[20] H. Ravanbod, "Application of neuro-fuzzy techniques in oil pipeline ultrasonic nondestructive testing," *NDT & E Int.*, vol. 38, no. 8, pp. 643–653, Dec. 2005.
[21] F. W. Margrave, K. Rigas, D. A. Bradley, and P. Barrowcliffe, "The use of neural network in ultrasonic flaw detection," *Measurement*, vol. 25, no. 2, pp. 143–154, 1999.
[22] T. D'Orazio, C. Guaragnella, M. Leo, and P. Spagnolo, "Defect detection in aircraft composites by using a neural approach in the analysis of thermographic images," *NDT & E Int.*, vol. 38, no. 8, pp. 665–673, Dec. 2005.
[23] D. P. Mandic, D. Obradovic, A. Kuh, T. Adali, U. Trutschell, M. Golz, P. De Wilde, J. Barria, A. Constantinides, and J. Chambers, "Data fusion for modern engineering applications: An overview," in *Proc. IEEE ICANN*, 2005, pp. 715–721.
[24] D. P. Mandic, M. Golz, A. Kuh, D. Obradovic, and T. Tanaka, *Signal Processing Techniques for Knowledge Extraction and Information Fusion*. New York: Springer-Verlag, 2008.
[25] Z. Xu, I. King, M. R. T. Lyu, and R. Jin, "Discriminative semi-supervised feature selection via manifold regularization," *IEEE Trans. Neural Netw.*, vol. 21, no. 7, pp. 1033–1047, Jul. 2010.
[26] H. Pan and L. Z. Xia, "Efficient object recognition using boundary representation and wavelet neural network," *IEEE Trans. Neural Netw.*, vol. 19, no. 12, pp. 2132–2149, Dec. 2008.
[27] J. S. Lim, "Finding features for real-time premature ventricular contraction detection using a fuzzy neural network system," *IEEE Trans. Neural Netw.*, vol. 20, no. 3, pp. 522–527, Mar. 2009.
[28] N. E. Huang, Z. Shen, S. R. Long, M. L. Wu, H. H. Shih, Z. Quanan, N. C. Yen, C. C. Tung, and H. H. Liu, "The empirical mode decomposition and the Hilbert spectrum for nonlinear and non-stationary time series analysis," *Proc. Roy. Soc. A*, vol. 454, no. 1971, pp. 903–995, Mar. 1998.
[29] G. Rilling, P. Flandrin, P. Goncalves, and J. M. Lilly, "Bivariate empirical mode decomposition," *IEEE Signal Process. Lett.*, vol. 14, no. 12, pp. 936–939, Dec. 2007.
[30] D. Looney, C. Park, P. Kidmose, M. Ungstrup, and D. P. Mandic, "Measuring phase synchrony using complex extensions of EMD," in *Proc. IEEE Stat. Signal Process. Symp.*, 2009, pp. 49–52.
[31] C. M. Sweeny-Reed and S. J. Nasuto, "A novel approach to the detection of synchronisation in EEG based on empirical mode decomposition," *J. Comput. Neurosci.*, vol. 23, no. 1, pp. 79–111, Aug. 2007.
[32] L. Cohen, "Instantaneous anything," in *Proc. IEEE ICASSP*, 1993, vol. 4, pp. 105–108.
[33] T. Tanaka and D. P. Mandic, "Complex empirical mode decomposition," *IEEE Signal Process. Lett.*, vol. 14, no. 2, pp. 101–104, Feb. 2007.
[34] M. U. Bin Altaf, T. Gautama, T. Tanaka, and D. P. Mandic, "Rotation invariant complex empirical mode decomposition," in *Proc. IEEE ICASSP*, 2007, vol. 3, pp. III-1009–III-1012.
[35] D. Looney and D. Mandic, "Multi-scale image fusion using complex extensions of EMD," *IEEE Trans. Signal Process.*, vol. 57, no. 4, pp. 1626–1630, Apr. 2009.
[36] P. Tass, M. G. Rosenblum, J. Weule, J. Kurths, A. Pikovsky, J. Volkmann, A. Schnitzler, and H.-J. Freund, "Detection of n:m phase locking from noisy data: Application to magnetoencephalography," *Phys. Rev. Lett.*, vol. 81, no. 15, pp. 3291–3294, Oct. 1998.
[37] Z. Wu and N. E. Huang, "Ensemble empirical mode decomposition: A noise-assisted data analysis method," Center for Ocean-Land-Atmosphere Studies, Calverton, MD, Tech. Rep. 193, 2004.
[38] I. T. Jolliffe, *Principal Component Analysis*. New York: Springer-Verlag, 2002.
[39] M. E. Tipping and C. M. Bishop, "Probabilistic principal component analysis," *J. Roy. Stat. Soc., Ser. B*, vol. 61, no. 3, pp. 611–622, 1999.
[40] A. Seghouanea and A. Cichocki, "Bayesian estimation of the number of principal components," *Signal Process.*, vol. 87, no. 3, pp. 562–568, Mar. 2007.
[41] T. P. Minka, "Automatic choice of dimensionality for PCA," in *Proc. Adv. NIPS*, 2000, pp. 598–604.

Marco Leo received the Honors degree in computer science engineering from the University of Lecce, Lecce, Italy, in 2001.

Since 2001, he has been a Researcher with the Institute of Intelligent Systems for Automation (ISSIA), Italian National Research Council (CNR), Bari, Italy. His main research interests are in the fields of image processing, image analysis, computer vision, pattern recognition, digital signal processing, neural networks, graphical models, wavelet transform, and independent component analysis. He participated in a number of national and international research projects facing automatic video surveillance of indoor and outdoor environments, human attention monitoring, real-time event detection in sport contexts, and nondestructive inspection of aircraft components. He is the author of more than 100 papers in national and international journals and conference proceedings. He is also a coauthor of three international patents on visual systems for event detection in sport contexts.

David Looney (M'11) received the B.Eng. degree in electronic engineering from University College Dublin, Dublin, Ireland, and the Ph.D. degree in statistical signal processing from Imperial College London, London, U.K., in 2011.

He is currently a researcher with the department of electrical and electronic engineering, Imperial College London. His research interests are mainly in the areas of adaptive data fusion, time–frequency analysis, and blind source separation.

Tiziana D'Orazio (M'08) received the Computer Science degree from the University of Bari, Bari, Italy, in 1988.

She held grants from the Italian National Research Council (CNR), Bari, from 1989 to 1993, for research activities in robotics and image processing. Since 1997, she has been a Researcher with the Institute of Intelligent Systems for Automation (ISSIA), CNR. His past activity was concerned with visual algorithms for autonomous navigation, artificial intelligence paradigm for elementary behavior learning, and feature extraction for pattern recognition. Her current research interests include pattern recognition, video analysis and computer vision for video surveillance, domotics, intelligent transportation systems, and quality control. She has published over 100 technical papers and book chapters in refereed conferences and journals in the areas of robotics and computer vision. She is a coauthor of three international patents on visual systems for event detection in sport contexts. She is also a frequent reviewer for leading conferences and journals.

Danilo P. Mandic (M'99–SM'03) received the Ph.D. degree in nonlinear adaptive signal processing from Imperial College London, London, U.K., in 1999.

He is currently a Professor in signal processing with Imperial College London. He has been working in the area of nonlinear adaptive signal processing and nonlinear dynamics. His publication record includes two research monographs titled *Recurrent Neural Networks for Prediction* (Wiley, 2001) and *Complex Valued Nonlinear Adaptive Filters: Noncircularity, Widely Linear and Neural Models* (Wiley, 2009), an edited book titled *Signal Processing for Information Fusion* (Springer, 2008), and more than 200 publications on signal and image processing. He has been a Guest Professor with Katholieke Universiteit Leuven, Leuven, Belgium; Tokyo University of Agriculture and Technology, Tokyo, Japan; and Westminster University, London. He has been a Frontier Researcher with RIKEN, Saitama, Japan. He has produced award-winning papers and products resulting from his collaboration with industry.

Prof. Mandic has been a member of the IEEE Technical Committee on Machine Learning for Signal Processing and an Associate Editor for the IEEE SIGNAL PROCESSING THEORY AND METHODS, IEEE TRANSACTIONS ON CIRCUITS AND SYSTEMS II, IEEE TRANSACTIONS ON SIGNAL PROCESSING, and IEEE TRANSACTIONS ON NEURAL NETWORKS. He is a member of the London Mathematical Society.